

See discussions, stats, and author profiles for this publication at: <https://www.researchgate.net/publication/281971162>

Real-Time Infrared–Mechano–Optical Behavior and Structural Evolution of Polypropylene and Hydroxyl-Functionalized Polypropylene during Uniaxial Deformation

ARTICLE *in* MACROMOLECULES · AUGUST 2015

Impact Factor: 5.8 · DOI: 10.1021/acs.macromol.5b01017

READS

32

5 AUTHORS, INCLUDING:



Ido Offenbach

University of Akron

4 PUBLICATIONS 5 CITATIONS

[SEE PROFILE](#)



Miko Cakmak

University of Akron

181 PUBLICATIONS 2,417 CITATIONS

[SEE PROFILE](#)

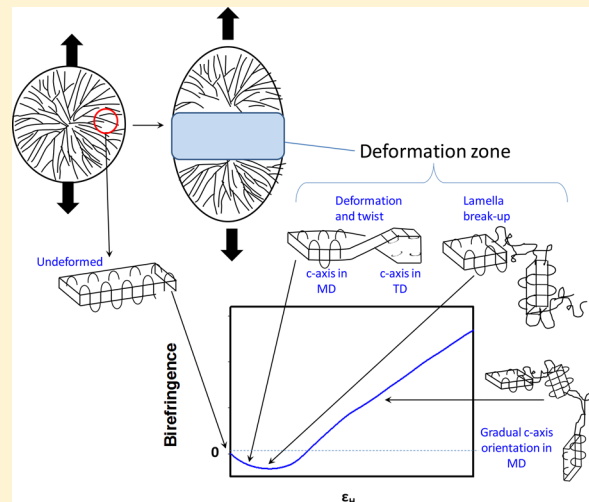
Real-Time Infrared–Mechano-Optical Behavior and Structural Evolution of Polypropylene and Hydroxyl-Functionalized Polypropylene during Uniaxial Deformation

I. Offenbach,[†] S. Gupta,[†] T. C. M. Chung,[‡] R. A. Weiss,[†] and M. Cakmak*,[†]

[†]Department of Polymer Engineering, The University of Akron, Akron, Ohio 44325, United States

[‡]Department of Materials Science and Engineering, The Pennsylvania State University, University Park, Pennsylvania 16802, United States

ABSTRACT: This paper focuses on the real-time mechano-optical behavior of hydroxyl-functionalized polypropylene (PPOH) copolymer containing 0.4 mol % comonomer of 10-hydroxy-1-undecene and its comparison with unmodified polypropylene (PP). The mechano-optical behavior of the two polymers was studied in the partially molten state during four different processing steps—heating, stretching, annealing, and cooling—with an integrated system that combined uniaxial stretching with real-time spectral birefringence and real-time ultrarapid-scan polarized FTIR measurements. While the material response was dominated by the crystalline network in both polymers, the presence of intermolecular hydrogen bonding between the hydroxyl groups was found to affect the structural evolution of the PPOH copolymer more significantly compared to the PP homopolymer. The PPOH copolymer exhibited not only lower crystallinity and smaller crystals but also a lower extent of lamella thickening at similar deformation conditions due to steric hindrance by the copolymer C9–side chains and OH groups. Uniaxial deformation of PP up to lower strains ($\epsilon_H \sim 0.1$) and subsequent cooling had the same effect on the crystal structure as annealing the polymer for longer times (≥ 30 min) at the same temperature with no deformation and subsequent cooling, which was a decrease in the population of smaller crystals and an increase in the average crystal size while maintaining similar crystallinity as the undeformed PP. Surprisingly, for PP both the amorphous and crystalline chain axes were oriented in the transverse direction (TD) at low strains before orienting in the machine direction (MD) at higher strains. However, no such observation was made for PPOH. This behavior was ascribed to the difference in breakup and unraveling of the spherulitic morphology between PP and PPOH upon deformation. In addition, four different regimes in the stress–optical curve were established for both the polymers. Stress relaxation immediately following uniaxial deformation of PP in the semimolten state resulted in a loss of MD orientation of crystalline segments but an increase in the MD orientation of amorphous segments. Unlike the result for PP, in PPOH the secondary H-bonded network supported the primary crystalline network during stress relaxation, and no change in the orientation of either crystalline or amorphous segments was observed. A schematic of the structural evolution was proposed based on the experimental results.



INTRODUCTION

Metalized biaxially oriented polypropylene (BOPP) represents the state-of-the-art in polymeric dielectric capacitors.^{1,2} Despite having the highest breakdown strength among polymers, which is 600–750 V/ μ m for $\sim 10\ \mu$ m thin films,^{3,4} BOPP provides an energy density of only $\sim 5\text{ J/cm}^3$ due to its low dielectric constant (~2.2). One of the methods to achieve a high dielectric constant is to incorporate functional polar groups that align in the direction of applied electric field and impart an additional mechanism of ionic polarizability in the polymer.^{3–5} Yuan et al.⁴ recently showed that the incorporation of only 4 mol % hydroxyl groups in polypropylene (PP) results in a 2-fold increase in the dielectric constant. Therefore, the hydroxyl-functionalized polypropylenes (PPOH) are of considerable

interest. Recent publications on the PPOH polymers have focused on the effect of hydroxyl groups on the thermal, structural, and rheological properties of PP⁶ and the crystallization kinetics and crystal morphology,⁷ all of which are important to consider during the melt-processing of PPOH polymers into thin films for capacitor application.

Thin polymeric capacitor films in the micrometer range are usually prepared by the tenter-frame biaxial stretching method. Tenter-frame biaxial stretching is a well-established technique^{8,9} where semicrystalline polymers, such as PP, are heated to a

Received: May 12, 2015

Revised: August 17, 2015

Published: August 21, 2015

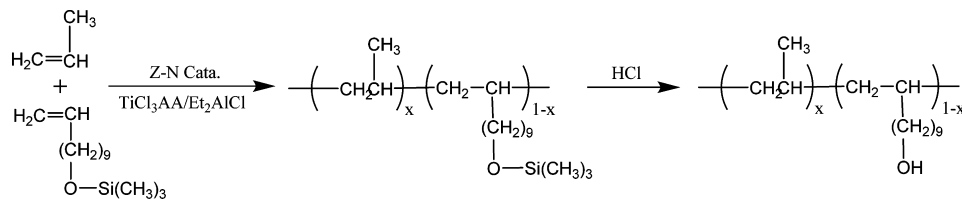


Figure 1. Synthesis of PPOH polymer.

semimolten state before stretching them in the machine direction (MD) followed by cooling and reheating and subsequent stretching in the transverse direction (TD). Therefore, the polymers are subjected to a complex thermomechanical deformation during a processing cycle of the tenter-frame biaxial stretching method.¹⁰ Moreover, the final state of polymer chain orientation and crystallinity is highly influenced by the processing conditions and dictate the final film properties and performance. While film tenter-frame biaxial stretching has been commercially employed for more than a decade, the structural evolution of polymer chains during such a process is still not well understood. Previously, we had reported on the real-time structural development of PP during uniaxial deformation in the partially molten state.^{11,12} In this paper, we report on the real-time structural development of a PPOH polymer and focus on the behavior of polymer chain segments separately in the amorphous and crystalline domains during heating, MD stretching, annealing, and cooling cycles of the tenter-frame biaxial stretching process. The results are compared with unmodified polypropylene.

EXPERIMENTAL DETAILS

Materials. Capacitor-grade PP homopolymer (Boreclean HB311BF) was donated by Borealis ($M_n = 53\,000$ g/mol, $M_w = 227\,000$ g/mol, $M_z = 529\,000$ g/mol, PDI = 4.2). PPOH polymer containing 0.4 mol % hydroxyl groups was synthesized by the Zeigler–Natta copolymerization reaction between propylene and undecenyl-oxytrimethylsilane comonomers, as shown in Figure 1. The synthesis procedure is described in detail elsewhere.⁴ The reactivity ratios for this copolymerization were $r_1 = 68$ for propylene and $r_2 = 0.032$ for the comonomer, due to which the chemical structure of the PPOH polymers was rather blocky than random.⁷

Sample Preparation. Unoriented polypropylene films were prepared in an extrusion casting line consisting of a Milacron extruder and a 12 in. wide slit die, casting rolls stack, six temperature- and motion-independent godet rolls, and a film collector. Table 1

summarizes the processing conditions along the casting line. A final thickness of 120 μm was obtained for the cast PP film. Unoriented PPOH films, 120 μm in thickness, were obtained by compression molding the polymer powder at 210 °C in a TMP Vacuum Compression Press. Dumbbell-shaped specimens were cut from both cast and molded films for further characterization.

Characterization. PP and PPOH specimens were uniaxially stretched in the partially molten state at various temperatures to 100% strain at a stretch rate of 15 mm/min. A real-time mechano-optical measurement platform equipped with an ultrarapid-scan polarized FTIR spectrometer was used to probe the deformation behavior of polymer segments in the crystalline and amorphous domains separately. Details of the measurement technique are discussed elsewhere.¹³ In brief, the specimen was clamped to load cells in the uniaxial stretching machine and enclosed within a thermal chamber. The stress-strain curves were calculated from the measured force and the true cross-sectional area of the deformed specimen, which was determined by measuring the real-time width of the specimen and assuming an incompressible deformation with transverse isotropy. This assumption has been checked in an earlier publication on polypropylene, and error committed was found to be within 4% of actual.¹⁵ The stress-strain data were further used to calculate the moduli of the PP and PPOH polymers. A visible wavelength light source and linear polarizers were used to measure the optical retardation (Γ) through the polymer specimen. The birefringence (Δn) was calculated from the ratio of optical retardation (Γ) and the true specimen thickness.

A disk mirror interferometer was used to measure infrared (IR) absorbance at a rate of 300 spectra per second. The IR beam was split into two components, one parallel and another perpendicular to the machine direction (MD), which allowed the calculation of Herman's orientation function (f_{IR}) using the equation¹⁴

$$f_{\text{IR}} = \frac{(D - 1)(D_0 + 2)}{(D + 2)(D_0 - 1)} \quad (1)$$

where D is the dichroic ratio, defined as the ratio of IR absorbance in parallel and perpendicular directions ($A_{||}/A_{\perp}$), and D_0 is the dichroic ratio of an ideally oriented polymer, defined as

$$D_0 = 2 \cot^2 \psi \quad (2)$$

where ψ is the transition moment angle of a specific side-group vibration with respect to the polymer chain axis.

The real-time mechano-optical measurements were made at four different processing steps in the following sequence: (1) preheating the polymer specimen from room temperature (RT) to the stretch temperature and 1 min of holding, (2) isothermal uniaxial stretching, (3) isothermal annealing for 30 min at the stretch temperature, and (4) cooling back to RT. The polymer specimen was confined between the clamps throughout these measurements.

The crystal structures were characterized with wide-angle X-ray diffraction (WAXD) and small-angle X-ray scattering (SAXS) on films stacked to provide sufficient thickness for good signal-to-noise ratio in data. WAXD measurements were performed using a Bruker AXS D8 goniometer, and SAXS measurements were performed using a Rigaku MicroMax002+ diffractometer. Both instruments used Cu $\text{K}\alpha$ radiation ($\lambda = 0.1542$ nm). SAXS was used to determine the long-spacing (L_p) of the crystals. WAXD diffractograms were used to measure any changes in the crystal structure of PP upon stretching and to compare the final values of orientation function with those obtained

Table 1. Processing Conditions for Preparing Unoriented Polypropylene Films

component	speed	temp (°C)
single screw extruder	zone 1	18.5 rpm
	zone 2	220
	zone 3	220
	zone 4	225
slit die		220
chiller rolls	1	1.8 m/min
	2	91
godet rolls	1	1.8 m/min
	2	120
	3	132
	4	130
	5	120
	6	95

from FTIR (f_{IR}). The Herman's orientation function was calculated from the WAXD data (f_{WAXD}) using the following equation for an α -monoclinic crystal structure of PP

$$f_{\text{WAXD}} = \frac{1}{2}(3\langle \cos^2 \theta_{c,z} \rangle - 1) \quad (3)$$

where $\theta_{c,z}$ is the angle between the c -axis and the stretch (z) direction (or MD). $\langle \cos^2 \theta_{c,z} \rangle$ was calculated using the equations¹²

$$\cos^2 \theta_{c,z} = 1 - 1.099 \cos^2 \theta_{110,z} - 0.901 \cos^2 \theta_{040,z} \quad (4)$$

$$\cos^2 \theta_{hkl,z} = \frac{\sum_{0^\circ}^{90^\circ} I_{hkl}(\theta) \sin \theta \cos^2 \theta}{\sum_{0^\circ}^{90^\circ} I_{hkl}(\theta) \sin \theta} \quad (5)$$

where $\theta_{hkl,z}$ is the angle between the normal to the (hkl) lattice plane and the stretch direction and 2θ is the Bragg's diffraction angle.

A TA Instruments differential scanning calorimeter (DSC Q-200) was used to measure the onset of melting ($T_{m,\text{onset}}$), melting point (T_m), and the heat of fusion (ΔH_f) of PP and PPOH films. Before the DSC measurements, temperature calibration was performed using an Indium standard ($T_m = 156.6^\circ\text{C}$). A heating rate of $10^\circ\text{C}/\text{min}$ was employed. The melting point was defined as the peak of the melting endotherm, with the largest peak denoted by T_m and the secondary peak denoted by T_m' . The melting onset temperature ($T_{m,\text{onset}}$) was measured at the point of intersection of the endotherm before the melting peak and the back-extrapolated curve from the endotherm after the melting peak. The back-extrapolation was done by a straight line with the same slope, i.e., heat capacity, as the endotherm after the melting peak. The mass fraction crystallinity of the polymer (ϕ_m) was calculated from the ratio of $\Delta H_f/\Delta H_{pp}$, where ΔH_f is the area under the DSC melting endotherm and ΔH_{pp} is the enthalpy of fusion of a 100% crystalline PP with an α -monoclinic structure, which is 165 J/g .¹⁵

In order to differentiate between the morphological changes that occurred in the polymers during each processing stage, DSC measurements were done separately on specimens that were sequentially removed from the uniaxial stretching chamber after each processing stage and subsequently cooled back to RT. These specimens are denoted as (heat-cool), (heat-anneal-cool), (heat-stretch-cool), and (heat-stretch-anneal-cool) in the text below.

RESULTS AND DISCUSSION

The thermal transitions for the PP and PPOH polymers are shown by the DSC endotherms in Figure 2. The addition of comonomer decreased the melting point (T_m) of PPOH by 10°C compared to PP, which is consistent with predictions from

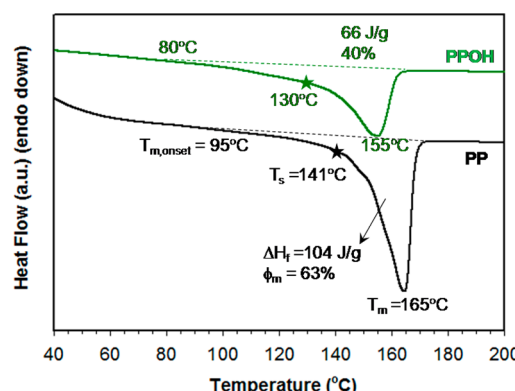


Figure 2. DSC curves for the PP and PPOH polymers obtained from the undeformed films. The symbols indicate the following: $T_{m,\text{onset}}$ = onset of melting, T_s = optimum stretching temperature determined from eq 6, T_m = melting point, ΔH_f = heat of fusion, and ϕ_m = mass fraction crystallinity of the polymer.

Flory's theory of melting-point depression in copolymers.¹⁶ The onset of melting ($T_{m,\text{onset}}$) also decreased for PPOH, by 15°C compared to PP, which is attributed to the decreased crystallizability and formation of smaller polypropylene crystals in the PPOH copolymer.⁶

An optimum temperature for stretching a semicrystalline polymer in the semimolten state (T_s) is typically determined using the relation¹²

$$T_s = T_m - \frac{1}{3}(T_m - T_{m,\text{onset}}) \quad (6)$$

The optimum stretching temperatures were calculated to be 141 and 130°C for PP and PPOH, respectively. In this study, we chose three deformation temperatures (T_d)— T_s , $T_s - 31$, and $T_s + 14$ —to cover a broad range of the semimolten regime based on the DSC exotherms in Figure 2.

Mechano-Optical Behavior. Heating to Deformation Temperatures. Figure 3 shows the stress development and Figure 4 shows the birefringence development in PP and PPOH films during the four stages of processing. In the first stage, the polymer film was heated to the deformation temperature (T_d) and isothermally maintained at that temperature for 1 min. Prior to the heating, the specimen was slightly stressed to prevent surface wrinkling and sagging during heating. The change in specimen length before and after heating was measured to be negligibly small. All the polymer specimens were completely relaxed before uniaxial stretching in the second stage, as indicated by a negligible stress at the deformation temperatures in Figure 3a. The average polymer chain orientation was isotropic before stretching as evidenced by the measured zero birefringence in Figure 4a.

The FTIR absorption spectra of the PP and PPOH polymers (not shown) were quite similar, except that PPOH showed two additional peaks at 3332 and 3637 cm^{-1} .⁶ The former corresponds to the stretching vibration of hydrogen-bonded OH groups, while the latter corresponds to the stretching vibration of non-hydrogen-bonded OH groups. The H-bond strength decreased upon increasing the deformation temperature.^{6,17} Figures 5a and 5b show the real-time evolution of vertically and horizontally polarized IR absorptions in the crystalline and amorphous regions of PP and PPOH polymers, respectively, during each of the four processing stages. The dichroic ratios (D, D_0) of crystalline and amorphous regions were calculated from the IR absorptions at 1045 and 2720 cm^{-1} , respectively.¹⁸ The vibrational modes at 1045 cm^{-1} are C-C stretching and C-CH₃ wagging with a crystalline transition dipole moment angle (ψ_c) of 0° .¹⁹ The transition dipole moment angle in the amorphous regions (ψ_a) is 90° . The orientation functions (f_{IR}) are shown in Figures 6 and 7 for PP and PPOH, respectively, at temperatures corresponding to $T_s - 31$ and $T_s + 14^\circ\text{C}$.

In the first heating stage, the orientation function was negligible for both amorphous (f_a) and crystalline (f_c) phases, which is consistent with the calculated birefringence in Figure 4a.

Although not much effect was observed on the polymer chain orientation upon heating the specimen to T_d and isothermally maintaining for a minute, changes in the crystal morphology occurred for both PP and PPOH as indicated by measurements of the crystallinity and the melting point. DSC exotherms measured on the heat-cool specimens are shown in Figure 8, and the values of ϕ_m and the melting points are summarized in Table 2.

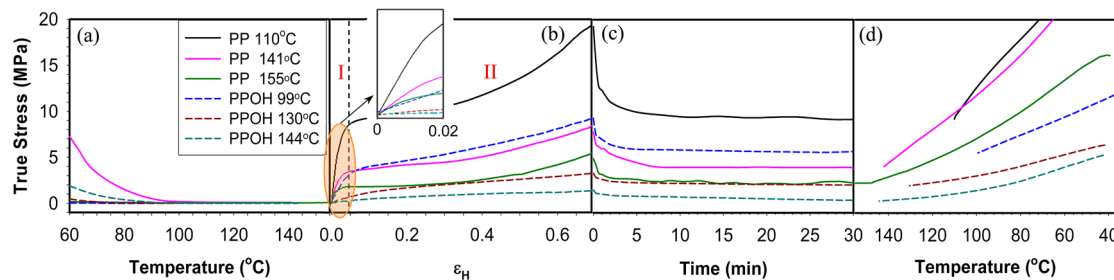


Figure 3. True stress of PP and PPOH at $T_s - 31\text{ }^\circ\text{C}$, T_s , and $T_s + 14\text{ }^\circ\text{C}$ during four stages of processing cycle: (a) heating + 1 min of holding, (b) stretching, (c) 30 min of annealing, and (d) cooling. Solid lines represent PP while the dashed lines represent PPOH. The stress–strain curve in the second stage can be divided into two regimes as shown for PP stretched at $110\text{ }^\circ\text{C}$, I = elastic flow and II = yielding and plastic flow. The inset in (b) shows the elastic deformation region.

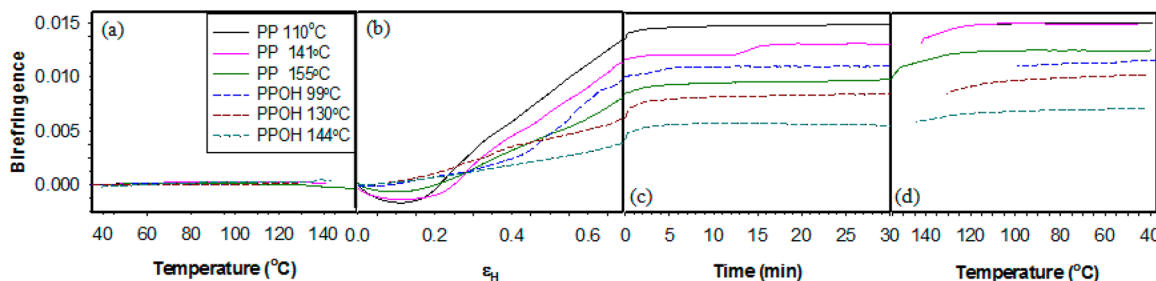


Figure 4. In-plane birefringence of PP and PPOH at $T_s - 31\text{ }^\circ\text{C}$, T_s , and $T_s + 14\text{ }^\circ\text{C}$ during four stages of processing cycle: (a) heating + 1 min of holding, (b) stretching, (c) 30 min of annealing, and (d) cooling. Solid lines represent PP while the dashed lines represent PPOH.

An existence of a second endothermic peak or shoulder (T_m') for heat–cool specimens indicated an increase in the crystal population of that size which would melt at the corresponding T_m' . Such an increase is attributed to lamella thickening which involves simultaneous melting of the smaller crystals (with $T_m \leq T_d$) and recrystallization of mobile amorphous segments onto the bigger crystals. Consequently, the onset of melting also increased with an increase in the deformation temperature, as shown in Figures 8 and 9a, although the melting point, T_m' , remained unchanged. The lamella thickening was also accompanied by an increase in the total crystallinity of heat–cool specimens compared to the unprocessed films. However, the exact state of crystallinity at T_d before cooling is unknown as it temporally changes.

The extent of lamella thickening, with $(T_m - T_m')$ as its measure, increased with the deformation temperature for both PP and PPOH, i.e., $(T_m - T_m')$ decreased at higher T_d as shown in Figure 9b. However, it was more pronounced in PP than PPOH at T_s or relative temperatures. Similar observations were made on the heat–anneal–cool polymer specimens that were heated to the deformation temperature and isothermally annealed for 30 min before cooling. Both the melting onset and the secondary melting temperature increased with the annealing temperature for PP and PPOH, with the extent of lamella thickening more pronounced in PP as shown in Figure 9b.

A direct evidence of lamella thickening was obtained from the SAXS measurements. Figure 10a shows the plots of the SAXS intensity (Iq^2 vs q , where q is the scattering wave vector) for heat–anneal–cool specimens of PP. The inset is the 2D SAXS profile for the heat–anneal–cool specimen of PP at $110\text{ }^\circ\text{C}$ which shows that the lamellar crystals were isotropically oriented. The long-spacing of lamellar crystals (L_p) was calculated using the equation

$$L_p = 2\pi/q_{\text{peak}} \quad (7)$$

where q_{peak} is the peak position in Figure 10a. The values of L_p are plotted in Figure 10b. For the heat–anneal–cool specimens, it was observed that the long-spacing was higher compared to the unprocessed film, increased with an increase in the annealing temperature, and was higher for PP compare to PPOH. These observations are consistent with the DSC measurements of the melting onset and the secondary melting point.

One of the possible reasons for a reduced lamellar thickening in PPOH polymer could be the steric hindrance from the copolymer side chains and the pendant hydroxyl groups that prevents periodic folding of the polypropylene backbone chains into a crystal structure. Interestingly, certain differences between the heat–cool and heat–anneal–cool specimens were observed. For example, in Figure 9b, the extent of lamella thickening decreased for the heat–anneal–cool specimens compared to the heat–cool specimens which indicated that melting became more pronounced than recrystallization upon prolonged exposure at the deformation temperatures.

Uniaxial Stretching. While not much difference was observed between PP and PPOH in the first heating stage in Figures 3a, 4a, 6a, and 7a, it was quite evident in the second stage where the polymer specimens were deformed uniaxially. The true stress–true (Hencky) strain curves at all deformation temperatures are shown in Figure 3b, and the calculated moduli data are given in Table 3. A typical behavior characteristic of a semicrystalline polymer was observed with an elastic deformation at lower strains (marked as regime I in Figure 3b) followed by yielding and necking (marked as regime II and separated by a dashed vertical line from regime I). The Young's modulus (E) and the yield strength (σ_y) naturally decreased upon increasing the deformation temperature.

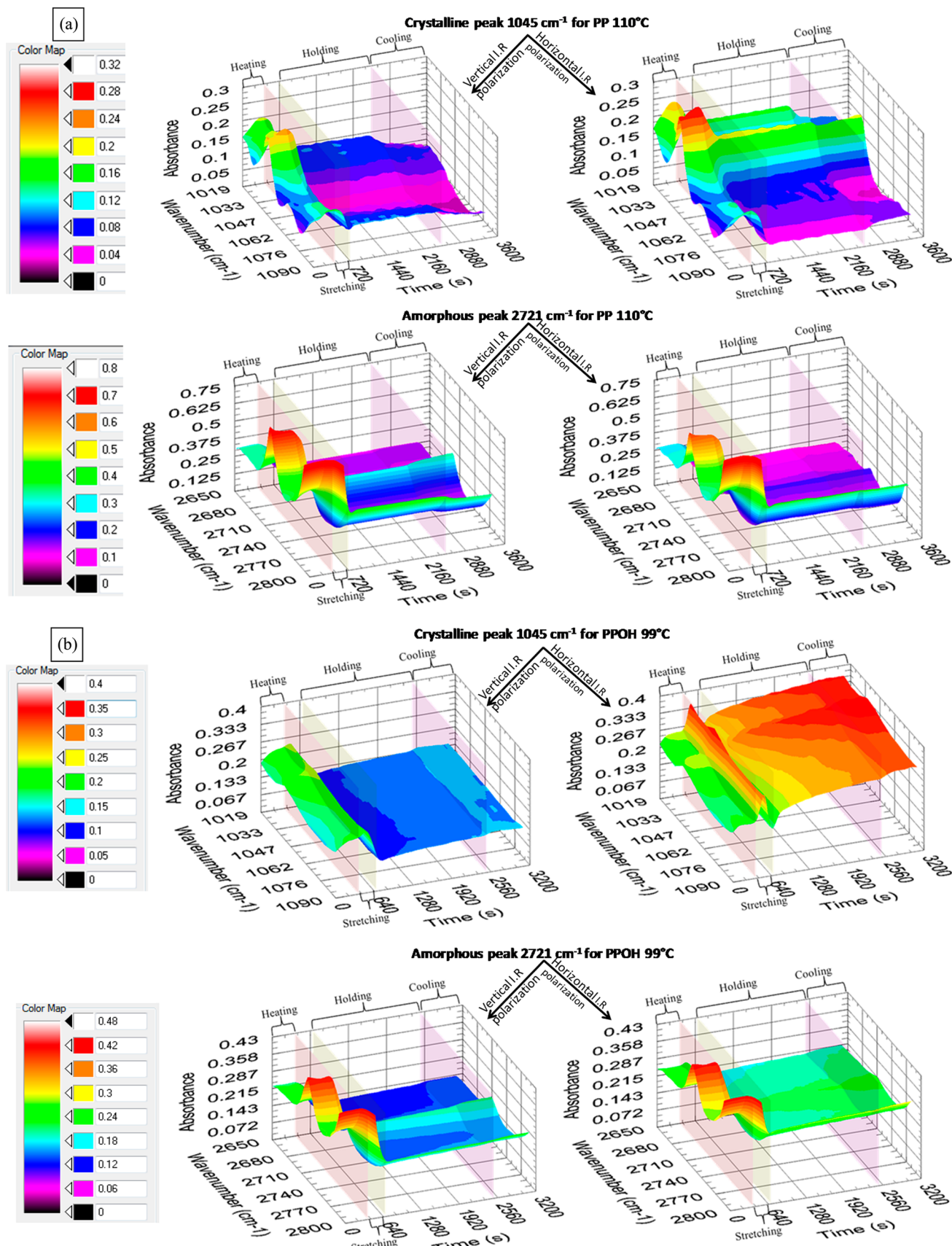


Figure 5. Real-time evolution of IR absorbance for the crystalline peak at 1045 cm^{-1} and the amorphous peak at 2721 cm^{-1} during the four stages of processing cycle (heating + 1 min holding, stretching, annealing, and cooling) for (a) PP processed 110 °C and (b) PPOH processed at 99 °C.

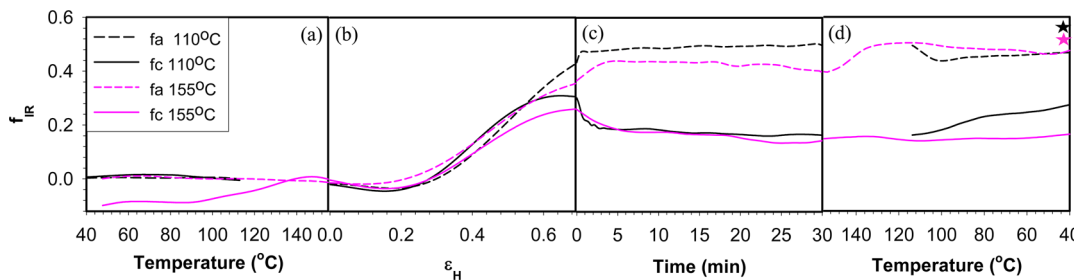


Figure 6. Orientation function of amorphous and crystalline segments in PP during the four stages of processing cycle: (a) heating + 1 min of holding, (b) stretching, (c) 30 min of annealing, (d) and cooling. The stars represent the crystalline orientation functions of the final samples at room temperature and calculated from offline WAXD measurements using eq 3.

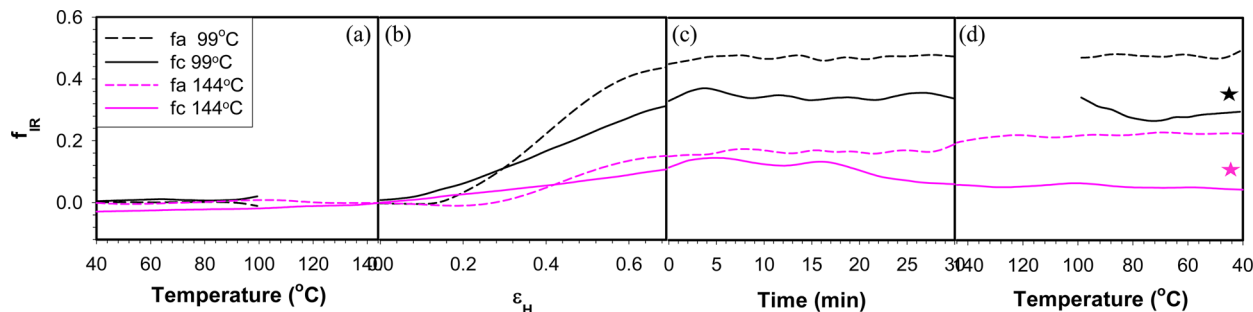


Figure 7. Orientation function of the amorphous and crystalline segments in PPOH during the four stages of processing cycle: (a) heating + 1 min of holding, (b) stretching, (c) 30 min of annealing, (d) and cooling. The stars represent the crystalline orientation functions of the final samples at room temperature and calculated from offline WAXD measurements using eq 3.

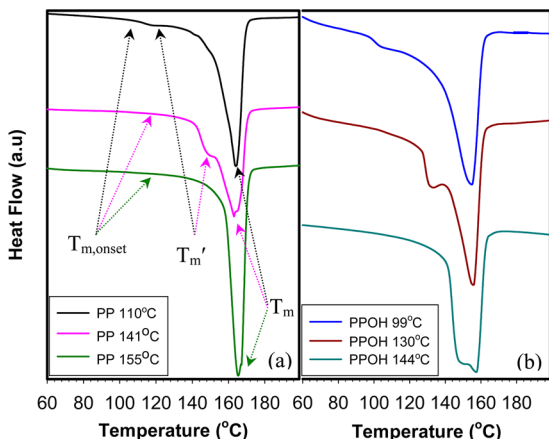


Figure 8. DSC endotherms for (a) PP and (b) PPOH after heating to the deformation temperature, holding for a minute, and cooling back to RT (heat-cool).

The contributions to the deformation stress in a semimolten state come from both the crystalline network and the trapped entanglements. The average entanglement spacing, represented by the tube diameter (a) in polymer reptation tube model, decreases upon decreasing the temperature.²⁰ Assuming that the incorporation of 0.4 mol % does not affect the entanglement spacing in PP, at the reference temperature of $T_s - \alpha_{PP}$ (141 °C) > α_{PPOH} (130 °C). This implies that the trapped entanglement contribution to the stress should be larger in PPOH than in PP at T_s . In addition, the PPOH polymer exhibited a higher melt elasticity and viscosity than PP⁷ due to intermolecular hydrogen-bonding interactions between the pendant OH groups, which is expected to require a further increase in the deformation stress in PPOH for a given strain. However, as observed in Figure 3b and Table 3, both the

Young's modulus and the yield strength were considerably lower for PPOH compared to PP at T_s or relative temperatures. Furthermore, yielding, which is associated with the unraveling of polymer chains from the lamellar crystals, occurred at lower strains in PP (see Table 3). These observations indicate that the material response in the semimolten state was dominated by the remaining crystalline network over that of H-bonding between the OH groups or the trapped entanglements and are consistent with a lower crystallinity of PPOH.

The differences in structural evolution between PP and PPOH during uniaxial stretching were also evident from the birefringence and FTIR measurements. The strain-optical curves shown in Figure 4b indicate that the orientation development at T_s or relative temperatures was higher in PP than PPOH, similar to the stress development. The average polymer chain orientation, with birefringence (Δn) as its measure, can be related to the crystalline and amorphous segmental orientations (f_c, f_a) and crystallinity (ϕ_m) using the two-phase model

$$\Delta n = f_c \phi_m \Delta n_c^0 + f_a (1 - \phi_m) \Delta n_a^0 + \Delta n_{\text{form}} \quad (8)$$

where Δn_c^0 and Δn_a^0 are the intrinsic birefringence of the polymer chains in the crystalline and amorphous phases, respectively, and Δn_{form} is the form birefringence which is assumed zero in the present case. Because of the exclusion of OH groups and comonomer side chains from the crystalline phase in the PPOH polymer,⁶ Δn_c^0 was considered to be equal for PP and PPOH. Also, considering the small comonomer content in the PPOH polymer, Δn_a^0 was assumed to be equal for PP and PPOH.

The birefringence data in Figure 4b were supplemented by the orientation functions of crystalline and amorphous phase, which are shown in Figures 6b and 7b for PP and PPOH, respectively. Both the amorphous and crystalline segment

Table 2. Thermal Properties of PP and PPOH Polymers before and after Each Processing Stage^a

Polymer	ϕ_m (%)	unprocessed film			deformation temperature			heat-cool			heat-anneal-cool			heat-stretch-anneal-cool						
		$T_{m,\text{onset}}$ (°C)	T_m' (°C)	T_m (°C)	T_d (°C)	ϕ_m (%)	$T_{m,\text{onset}}$ (°C)	T_m' (°C)	T_m (°C)	$T_{m,\text{onset}}$ (°C)	ϕ_m (%)	$T_{m,\text{onset}}$ (°C)	T_m' (°C)	T_m (°C)	ϕ_m (%)	$T_{m,\text{onset}}$ (°C)	T_m' (°C)	T_m (°C)		
PP	63	95	165	$T_s - 31$	110	66	103	125	164	67	106	133	165	48	122	155	164	61	114	
			T_s	141	67	108	150	164	63	112	144	164	50	136	161	165	68	123	163	
			$T_s + 14$	155	68	115		165	65	116	162	165	58	148	163	165	69	127	164	
PPOH	40	80	155	$T_s - 31$	99	42	82	105	155	44	92	104	158	39	93	110	157	43	86	103
			T_s	130	47	96	133	156	38	98	130	157	30	108	145	156	49	106	132	
			$T_s + 14$	144	45	96	149	157	39	110	145	157	34	119	149	157	53	110	147	

^aThe measurement errors in crystallinity (ϕ_m) are $\pm 2\%$, melting onset ($T_{m,\text{onset}}$) are $\pm 2^\circ\text{C}$, and T_m' and T_m are $\pm 1^\circ\text{C}$.

orientation gradually increased in the direction of deformation from an unoriented state, which is consistent with the birefringence measurements. However, a few differences were observed between PP and PPOH. First, a slightly negative birefringence was measured in PP up to a Hencky strain of ~ 0.16 (see Figure 4b), during which the polymer had already transitioned from an elastic to a plastic deformation regime. Afterward, the birefringence gradually increased to zero and became positive. The magnitude of negative birefringence was highest at the lowest deformation temperature. This observation is supported independently by the data in Figure 6b where both the amorphous and crystalline orientation functions become slightly negative at the beginning of deformation before increasing to a positive value.

The individual contributions from the crystalline and amorphous phases to the overall birefringence during uniaxial stretching of polymers have been previously reported. Samuels²¹ observed that the orientation function of the amorphous phase during uniaxial stretching of PP was negative; i.e., amorphous PP chains were oriented in the TD at strains up to 100%, beyond which it became positive. This was found true for both compression-molded and cast-and-annealed samples. However, unlike the results reported in this study, the crystalline orientation functions and the overall birefringence were measured to be always positive. On the contrary, Sasaguri et al.²² showed that PP exhibits a negative birefringence upon uniaxially stretching at low strains after aging for several days. This is attributed to the negative contributions from the crystalline phase. Opposite to the observations by Samuels and Sasaguri et al., other studies^{23,24} on uniaxial stretching of PP show a positive amorphous and crystalline orientation functions.

The results obtained in Figures 4b, 6b, and 7b indicate that the spherulitic deformation in PP at the beginning of uniaxial extension results in a morphology where a fraction of the individual lamellae become aligned toward the MD with crystalline segments comprising the lamellae oriented toward the TD. One of the mechanisms through which this is possible is the lamellar bending, twisting, and splaying within the equatorial planes of spherulites followed by the lamellar breakup. Similar models have been proposed for polyethylene deformation by Shimamura et al.²⁵ and Michler et al.²⁶ based on SEM and TEM observations, respectively, and for polybutene-1 deformation by Sasaguri et al.²⁷ As a consequence of this morphology, the interlamellae tie chains in the amorphous phase may also be forced to orient in the TD. Upon further deformation of the polymer specimen beyond the elastic regime, the amorphous tie chains and those unraveled from the crystalline regions during necking gradually orient in the MD. This is simultaneously followed by further lamellar breakup and their rotation in TD along their length, which results in the crystalline segments comprising the lamellae to orient in the MD. The above result is also consistent with AFM observations of crystalline morphology in a polyamide film subjected to uniaxial deformation.²⁸

Contrary to PP, such an observation was not made for the PPOH polymer in Figure 4b or 7b. It appears that the crystal lamellae in PPOH bear the initial load during uniaxial deformation. This was evident from a zero f_a but a nonzero positive f_c in Figure 7b during the initial deformation. A nonzero positive f_c indicates that the spherulitic breakup in PPOH commenced by rotation of the lamellae in the TD which resulted in the MD orientation of crystalline segments. The

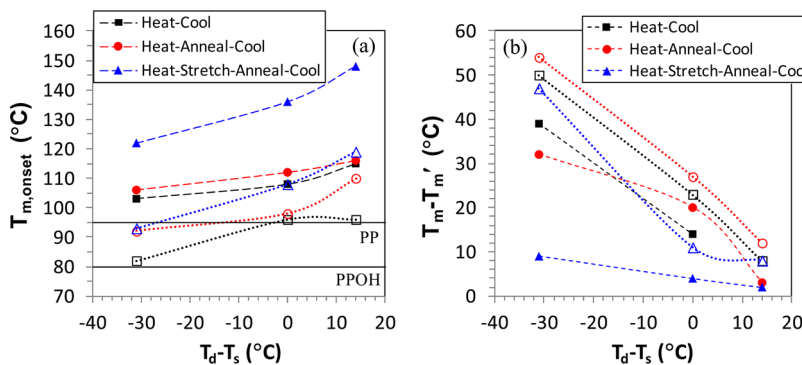


Figure 9. (a) Onset of melting and (b) difference between the primary and secondary melting temperatures as a measure of lamella thickening, for PP (filled symbols, dashed lines) and PPOH (open symbols, dotted lines) polymers subjected to different deformation temperatures. The lines are drawn for clarity.

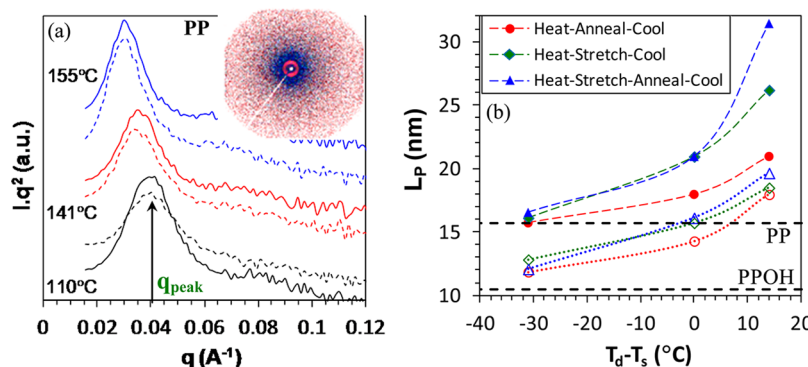


Figure 10. (a) SAXS intensity profile as a function of the scattering wave vector. Solid curves correspond to heat-anneal-cool specimens of PP. Dotted curves correspond to specimens that were stretched until the point of minimum birefringence in Figure 4b and cooled. The curves are shifted vertically for clarity. The inset is a 2D profile for the heat-anneal-cool specimen of PP at 110 °C, indicating random orientation. (b) Long-spacing of lamellar crystals of PP (filled symbols, dashed lines) and PPOH (open symbols, dotted lines) subjected to different deformation temperatures. The lines are drawn for clarity. The long-spacing of underformed PP and PPOH is shown by the horizontal dashed lines.

Table 3. Mechanical Properties of PP and PPOH Polymers^a

polymer	T_d (°C)	E (MPa)	σ_y (MPa)	ε_y	$C'_0 \times 10^3$ (MPa $^{-1}$)				σ_{rel} (MPa)	
					I	II	III	IV		
PP	$T_s - 31$	110	358.2	8.8	0.06	-0.11	-0.63	6.18	1.48	9.2
	T_s	141	150.4	3.4	0.05	-0.16	-0.93	11.95	2.17	3.5
	$T_s + 13$	155	117.5	1.8	0.05	-0.27	-5.97	5.84	1.61	2.2
PPOH	$T_s - 31$	99	70.6	3.8	0.08	-0.02	1.03	2.87	1.82	3.4
	T_s	130	10.0	1.4	0.13	0.28	3.02	4.88	2.61	1.1
	$T_s + 13$	144	4.5	0.5	0.13	0.50	3.22	7.12		0.6

^a T_d = deformation temperature, E = Young's modulus, σ_y = yield strength, ε_y = yield (Hencky) strain, C'_0 = photoelastic coefficient, and σ_{rel} = stress relaxed.

amorphous tie chains were negligibly affected during this process.

Although the reasons for this different behavior of PP and PPOH are not clear, one of the plausible reasons could be the coarser spherulitic morphology of the PPOH polymer with lower crystallinity.⁷

The stress-optical curves for the stretching stage are shown in Figure 11 for PP and PPOH. Analogous curves for the orientation function vs stress for PP and PPOH are shown in Figures 12a and 12b, respectively. In general, four regimes with different photoelastic coefficients (C'_0) could be distinguished, as marked in Figure 11 for PP stretched at 110 °C. The values of C'_0 are given in Table 3. In the first regime, which is characterized by elastic deformations at low strains in Figure 3b,

birefringence in PP became negative and that in PPOH became positive (except at 99 °C where it was negligibly small), indicating different mechanisms of spherulitic breakup, as discussed previously. As evident from Figure 12a,b, this is caused by a negative f_c and a negative f_a for PP but a positive f_c and zero f_a for PPOH. In the second regime which is characterized by a transition from elastic deformation to yielding and commencement of necking in Figure 3b, C'_0 further decreased for PP and increased for PPOH, indicating further growth of the bulk morphology observed in regime I.

The third and fourth regimes in Figure 11 were characterized by neck propagation in Figure 3b. In the third regime, a sudden increase in birefringence was observed for both PP and PPOH. The presence of such a "stress offset" in the development of

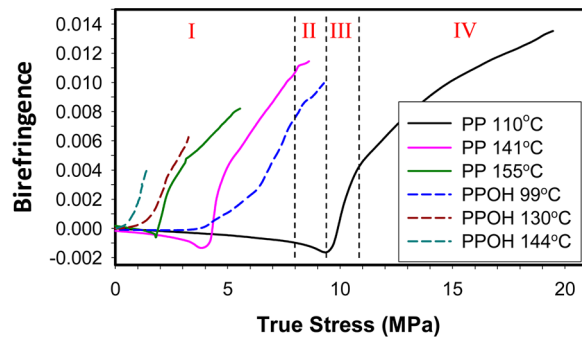


Figure 11. Stress-optical curves for PP and PPOH polymers at different deformation temperatures for the stretching stage. Different regimes for PP stretched at 110 °C are marked and separated by the dotted lines.

optical anisotropy is consistent with previous observations in semicrystalline^{12,29} polymers stretched in the semimolten regime as well as amorphous³⁰ polymers stretched near the T_g . As evident from Figure 12a,b, the rate of orientation development in this regime was almost equal for both amorphous and crystalline segments in PP but was higher for the amorphous than crystalline segments in PPOH. In the fourth regime, C_0 decreased slightly compared to the third regime which could be attributed to the gradual saturation in polymer chain orientation as they approach their limit of extensibility.

An interesting observation from Figure 11 is that the stress offset for birefringence development decreased upon increasing the deformation temperature for both PP and PPOH and was higher for PP than PPOH at relative deformation temperatures. However, the strain offset (calculated from Figure 3b as the strain at the stress offset) varied only slightly between PP and PPOH, extended into the plastic deformation regime, and was independent of the deformation temperature (Figure 4b). This universality of the strain offset suggests that the orientation of polymer chains in the direction of deformation was mainly restricted by the process of yielding, and that the stress merely scaled inversely with the temperature.

Thermal Annealing and Cooling. The uniaxial deformation was followed by thermal annealing in the third stage where the stretched specimen was kept fixed between the clamps at the stretching temperature for 30 min. Even in this stage, differences in the structural evolution between PP and PPOH were observed. Figure 3c shows the stress evolution, Figure 4c

shows the change in birefringence, and Figures 6c and 7c show the change in orientation functions for PP and PPOH, respectively, as a function of annealing time. Stress relaxation was observed in all cases; however, the stress did not relax back to zero but leveled off at an arbitrary value. The value of the total stress relieved upon annealing (σ_{rel}) is given in Table 2. Interestingly, σ_{rel} was very close to the yield stress (σ_y), suggesting that the major contributions to the stress relaxation come from the “elastic” motions and only minor contributions may come from the large-scale segmental motion or reptation of the polymer chains.

The birefringence increased only slightly upon annealing, which was consistent with the orientation function measurements. For PP, the crystalline orientation function decreased and the amorphous orientation function increased for early annealing times up to 3 min before stabilizing to a constant value and, hence, no significant change in the overall birefringence. The occurrence of thermal crystallization at the annealing temperature would be expected to produce MD-oriented crystalline segments due to MD-oriented amorphous chains, thereby increasing the f_c , which is not observed in Figure 6c. Also, in such a case, one would expect the relaxation time scale to be temperature dependent, which is again not observed from Figure 6c. One of the possibilities for a decrease in f_c could be the relaxation resulting from the minor spatial rotation of oriented lamellar crystals as a mechanism of stress release. The amorphous tie chains that are trapped between the crystalline junctions can only undergo limited reptation but can relieve stresses by axial rotation of the strained bonds. The spatial rotation of the lamellar crystals and the strained bonds is also consistent with the “elastic” nature of stress relaxation and, combined with limited reptation of amorphous chains, may result in $\sigma_{rel} > \sigma_y$.

In contrast to PP, smaller changes in the amorphous orientation function or the crystalline orientation function were observed for PPOH in Figure 7c, and $\sigma_{rel} < \sigma_y$ from Table 2 (except PPOH annealed at 144 °C), indicating that the elastic stress imposed during uniaxial deformation was not fully recovered. Both these results can be attributed to a more complex semicrystalline morphology of the PPOH polymer compared to PP due to the presence of H-bonding,⁷ which increases the viscosity and inhibits segmental motion of the polymer chains.

Cooling the stretched and annealed polymer specimen from deformation temperatures back to room temperature in the

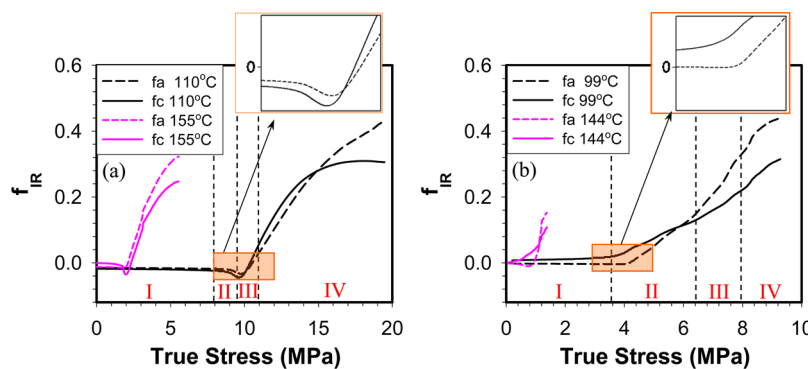


Figure 12. Orientation functions for crystalline and amorphous polymer chain segments as a function of true stress for (a) PP and (b) PPOH at different deformation temperatures. Different regimes corresponding to Figure 11 are marked and separated by the dotted lines for (a) PP stretched at 110 °C and (b) PPOH stretched at 99 °C. The inset is a magnification of the selected area on the plot.

fourth stage led to an increase in the stress (Figure 3d), primarily due to thermal shrinkage of the specimens which were still spatially confined between the clamps in the machine direction but free to contract in transverse directions. For both polymers, the thermal stresses were higher but the percent increase was lower upon cooling from a lower deformation temperature. The increase in stress was larger for PP than PPOH, which can be attributed to the higher crystallinity of PP analogous to creating more physical cross-linked joints inside the polymer. Birefringence measurements in Figure 4d showed that the polymer chain orientation did not change much upon cooling, which is consistent with a negligible change in the orientation functions, f_a and f_c , in Figures 6d and 7d for PP and PPOH, respectively.

Stretching and annealing the polymer specimen at different deformation temperatures also resulted in a change in the crystallinity and the secondary melting point; see Table 2 (heat–stretch–anneal–cool). In order to decouple the effect of stretching from annealing on ϕ_m and T_m' , DSC measurements were performed on the specimens that were cooled immediately after stretching. These values are given in Table 2 (heat–stretch–cool). For the heat–stretch–cool specimens, the crystallinity was higher than the unprocessed film and increased with an increase in the deformation temperature for both PP and PPOH. Since stretching up to high strains is expected to break lamellar crystals and reduce crystallinity, an increase in the crystallinity of both PP and PPOH was surprising. In conjunction with the crystallinity, the long spacing also increased with the deformation temperature (refer to Figure 10b), with simultaneous increases in $T_{m,\text{onset}}$ and T_m' in Table 2. In light of this observation, it is reasonable to postulate that stretching of the polymer specimen breaks the smaller crystals first before breaking the larger ones. When the stretching is stopped and the polymer cooled, thermal crystallization occurs where the molten polymer chains crystallize on the existing lamellar crystals. Cooling from a higher temperature provides more time for polymer chains to crystallize; hence, ϕ_m , L_p , $T_{m,\text{onset}}$, and T_m' increase with an increase in the deformation temperature. Clearly, thermodynamically driven lamella thickening occurs at the expense of smaller crystals. It is interesting to note that the average long spacings in the PP specimens that were stretched up to the point of lowest birefringence and cooled were the same as those for the heat–anneal–cool specimens (see Figure 10a).

Similar lamella thickening was observed for the heat–stretch–anneal–cool specimens as well. Their crystallinity were lower than the heat–stretch–cool specimens, which is consistent with previous observations of a lower crystallinity of heat–anneal–cool specimens compared to heat–cool specimens (refer to Table 2). Both of these results suggest that melting is more pronounced than recrystallization upon prolonged annealing at the deformation temperatures. The total crystallinity of heat–stretch–anneal–cool specimens of PP increased with an increase in T_d whereas that for PPOH decreased, but it was lower than the unprocessed film for both the polymers. A decrease in ϕ_m with an increase in T_d for PPOH was also observed for the heat–anneal–cool specimens and can be attributed to the steric hindrance by the copolymer side chains and the pendant OH groups to the regular folding of PP chains into a crystal structure while the polymer was cooling back to room temperature.

Crystal Structure. The crystalline orientation function calculated from FTIR measurements was confirmed independ-

ently with WAXD measurements. Figure 13 shows the WAXD diffractograms for PP and PPOH at the end of the processing

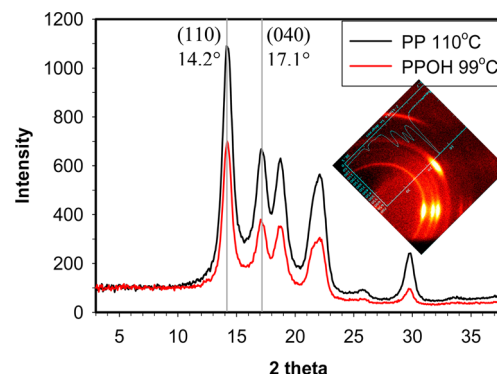


Figure 13. Wide-angle X-ray diffractograms of PP and PPOH polymers after a full processing cycle (heating + 1 min holding, stretching, annealing, and cooling). The inset shows a 2D WAXD pattern of PP stretched at 110 °C.

cycle. No change was observed in the crystal structure of both polymers, which was an α -monoclinic polypropylene crystal.^{31,32} The Hermans orientation function (f_{WAXD}) was calculated using eqs 3–5 based on the (110) and (040) lattice planes. The calculated values are compared with f_{IR} in Figures 6d and 7d and were fairly close for PPOH but higher for PP.

Structural Evolution. Based on the above results and discussions, a schematic is provided in Figure 14 for the structural evolution of polypropylene homopolymer during uniaxial stretching in the partially molten state focusing on why we observe negative birefringence during real time stretching of PP. Within the partially molten regime (i.e., between $T_{m,\text{onset}}$ and T_m'), both the melting and recrystallization process are occurring dynamically. Based on the previous^{25–28} and current results, the deformation of spherulitic structures tends to start in the equatorial regions of the spherulites. Lamella twisting occurs first, followed by the lamella breakup and rotation. This latter mechanism leads to crystalline chains in the lamellae orient perpendicular to the stretching direction. Since the PP chains exhibit positive intrinsic birefringence ($\Delta n_c^0 = 0.0331$, $\Delta n_a^0 = 0.0468$),²¹ initially optically isotropic material temporarily exhibits negative birefringence ($n_{\text{TD}} > n_{\text{MD}}$). With further increase in deformation, the chains unraveling from the lamellae begin to more substantially orient in the machine direction to eventually reverse this trend, and the birefringence becomes positive.

CONCLUSIONS

The structural evolution of polypropylene during heating, uniaxial stretching, annealing, and cooling was studied, and the effect of incorporation of 0.4 mol % comonomer of 10-hydroxy-1-undecene in PP was investigated. The mechano-optical behavior was primarily dominated by the crystalline morphology but was influenced by the presence of intermolecular H-bonding and the C9 side chains of the copolymer. Independent and simultaneous measurements of the in-plane birefringence and orientation functions of the amorphous and crystalline segments shed light on the behavior of the polymer segments during each stage of the deformation. The breakup of spherulite morphology at the early stages of uniaxial deformation was found to be different for PP as compared to PPOH. In PP, the spherulitic breakup led to breakup and rotation of lamellae

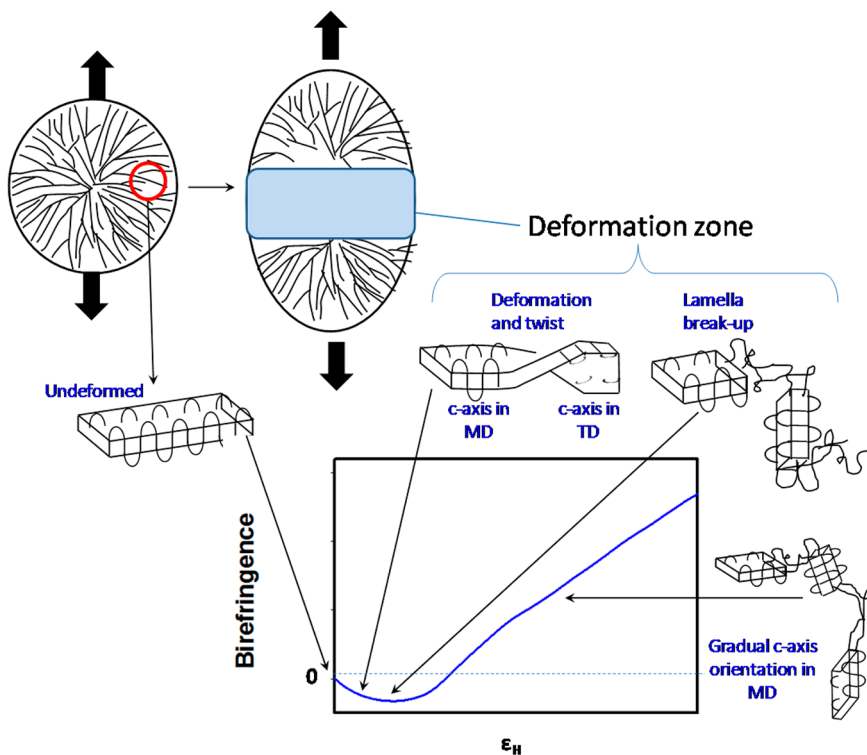


Figure 14. Schematic depicting the structural evolution of polypropylene during uniaxial stretching from the partially molten state.

fragments in the equatorial regions of the spherulites first, with this rotation leading to observation of a negative birefringence. Further stretching reversed this trend, and thus the birefringence sign became positive as the amorphous and crystalline chains attained increasingly large preferential orientation in the MD. This initial negative birefringence was not observed in PPOH. Four different regimes in the stress-optical curve for uniaxial deformation were observed for both polymers and explained on the basis of changes in crystal morphology. An increase in the polymer chain orientation in the MD was always preceded by a stress offset that decreased with an increase in the deformation temperature. Growth of a second crystal population and lamella thickening was observed in most cases for both PP and PPOH polymers. However, the crystal size was always lower for PPOH due to steric hindrance by the hydroxyl groups and the copolymer side chains.

AUTHOR INFORMATION

Corresponding Author

*E-mail: cakmak1@uakron.edu (M.C.).

Present Address

S.G.: Parker Hannifin Corporation, Parflex Division, 1300 N. Freedom St., Ravenna, OH 44266.

Author Contributions

I.O. and S.G. contributed equally.

Notes

The authors declare no competing financial interest.

ACKNOWLEDGMENTS

Financial support for this work through a Multidisciplinary University Research Initiative (MURI) grant from the Office of Naval Research (Contract No. N00014-10-1-0944) is greatly appreciated.

REFERENCES

- (1) Barshaw, E. J.; White, J. J.; Chait, M. J.; Cornette, J. B.; Bustamante, J.; Folli, F.; Biltchick, D.; Borelli, G.; Picci, G.; Rabuffi, M. *IEEE Trans. Magn.* **2007**, *43*, 223–225.
- (2) Rabuffi, M.; Picci, G. *IEEE Trans. Plasma Sci.* **2002**, *30*, 1939–1942.
- (3) Wang, C. C.; Ramprasad, R. *J. Mater. Sci.* **2011**, *46*, 90–93.
- (4) Yuan, X.; Matsuyama, Y.; Chung, T. C. M. *Macromolecules* **2010**, *43*, 4011–4015.
- (5) Lorenzini, R. G.; Kline, W. M.; Wang, C. C.; Ramprasad, R.; Sotzing, G. A. *Polymer* **2013**, *54*, 3529–3533.
- (6) Gupta, S.; Yuan, X.; Chung, T. C. M.; Kumar, S.; Cakmak, M.; Weiss, R. A. *Macromolecules* **2013**, *46*, 5455–5463.
- (7) Gupta, S.; Yuan, X.; Chung, T. C. M.; Cakmak, M.; Weiss, R. A. *Polymer* **2014**, *55*, 924–935.
- (8) Kahn, H. A.; Henze, E. D. Process for production of biaxially. US3223764A, 1965.
- (9) Jolliffe, C. N. Method of making biaxially oriented thermoplastic films. US5429785A, 1995.
- (10) Cole, K. C.; Depecker, C.; Jutigny, M.; Lefebvre, J.-M.; Krawczak, P. *Polym. Eng. Sci.* **2004**, *44*, 231–240.
- (11) Koike, Y.; Cakmak, M. *Macromolecules* **2004**, *37*, 2171–2181.
- (12) Koike, Y.; Cakmak, M. *Polymer* **2003**, *44*, 4249–4260.
- (13) Unsal, E.; Nugay, I. I.; Offenbach, I.; Gross, M.; Manning, C.; Cakmak, M. *Rev. Sci. Instrum.* **2013**, *84*, 073901.
- (14) Flory, P. J. *Trans. Faraday Soc.* **1954**, *51*, 848–857.
- (15) Wunderlich, B. *Macromolecular Physics*; Academic Press: New York, 1980; Vol. 3, p 63.
- (16) Samuels, R. J. *J. Chem. Phys.* **1958**, *28*, 1113–1115.
- (17) Gupta, S.; Yuan, X.; Chung, T. C. M.; Cakmak, M.; Weiss, R. A. Unpublished results.
- (18) Samuels, R. J. *Makromol. Chem.* **1981**, *4*, 241–270.
- (19) McDonald, M. P.; Ward, I. M. *Polymer* **1961**, *2*, 341–355.
- (20) Fetter, L. J.; Lohse, D. J.; Richter, D.; Witten, D. A.; Zirkel, A. *Macromolecules* **1994**, *27*, 4639–4647.
- (21) Samuels, R. J. *J. Polym. Sci., Part A: Gen. Pap.* **1965**, *3*, 1741–1763.

- (22) Sasaguri, K.; Hoshino, S.; Stein, R. S. *J. Appl. Phys.* **1964**, *35*, 47–54.
- (23) Song, Y.; Nitta, K.; Nemoto, N. *Macromolecules* **2003**, *36*, 1955–1961.
- (24) Bao, R.; Ding, Z.; Zhong, G.; Yang, W.; Xie, B.; Yang, M. *Colloid Polym. Sci.* **2012**, *290*, 261–274.
- (25) Shimamura, K.; Murakami, S.; Katayama, K. *Makromol. Chem., Rapid Commun.* **1982**, *3*, 199–204.
- (26) Michler, G. H. *Colloid Polym. Sci.* **1992**, *270*, 627–638.
- (27) Sasaguri, K.; Yamada, R.; Stein, R. S. *J. Appl. Phys.* **1964**, *35*, 3188–3194.
- (28) Drechsler, D.; Karbach, A.; Fuchs, H. *Surf. Interface Anal.* **1997**, *25*, 537–542.
- (29) Onogi, S.; Asada, T.; Tanaka, A. *J. Polym. Sci. A-2* **1969**, *7*, 171–182.
- (30) Muller, R.; Pesce, J. *Polymer* **1994**, *35*, 734–739.
- (31) Rabiej, S.; Wlochowicz, A. *Angew. Makromol. Chem.* **1990**, *175*, 81–97.
- (32) Agarwal, P. K.; Soman, R. H.; Weng, W.; Mehta, A.; Yang, L.; Ran, S.; Liu, L.; Hsiao, B. S. *Macromolecules* **2003**, *36*, 5226–5235.